Impact of thermal annealing on photoacoustic response and heat transport in porous silicon based nanostructured materials

Pavlo Lishchuk, Ali Belarouci, Roman Tkach, Kateryna Dubyk, Roman Ostapenko, Vasyl Kuryliuk, Guillaume Castanet, Svitlana Naumenko, Andrey Kuzmich, Fabrice Lemoine, et al.

Impact of thermal annealing on photoacoustic response and heat transport in porous silicon based nanostructured materials

Cite as: AIP Conference Proceedings **2170**, 020008 (2019); https://doi.org/10.1063/1.5132727
Published Online: 05 November 2019

Pavlo Lishchuk, Ali Belarouci, Roman Tkach, Kateryna Dubyk, Roman Ostapenko, Vasyl Kuryliuk, Guillaume Castanet, Svitlana Naumenko, Andrey Kuzmich, Fabrice Lemoine, Vladimir Lysenko, David Lacroix, and Mykola Isaiev

Impact of Thermal Annealing on Photoacoustic Response and Heat Transport in Porous Silicon Based Nanostructured Materials

Pavlo Lishchuk[1, a)], Ali Belarouci[2], Roman Tkach[2,3], Kateryna Dubyk[1], Roman Ostapenko[1], Vasyl Kuryliuk[1], Guillaume Castanet[4], Svitlana Naumenko[1], Andrey Kuzmich[1], Fabrice Lemoine[4], Vladimir Lysenko[2], David Lacroix[4] and Mykola Isaiev[4, 1 b)]

[1]*Faculty of Physics, Taras Shevchenko National University of Kyiv, 64/13, Volodymyrska Str., Kiev 01601, Ukraine.*
[2]*Université de Lyon; Institut des Nanotechnologies de Lyon, UMR-5270, Ecole Centrale de Lyon, Ecully, France*
[3]*National Technical University of Ukraine 'Kyiv Polytechnic Institute', Physical Engineering Faculty, 35, Politekhnichna Str., 03056 Kyiv, Ukraine*
[4]*Universite de Lorraine, CNRS, LEMTA, Nancy, F-54000, France*

[a)] pavel.lishchuk@gmail.com
[b)] Corresponding author: mykola.isaiev@univ-lorraine.fr

Abstract. Features of heat transport in silicon-based porous structures with different morphology before and after thermal annealing are investigated. Specifically, fractal-like porous silicon and silicon nanowire arrays samples were considered. All the structures were annealed in dry air at various temperatures in diapason from 600 °C up to 1000 °C for 20 minutes. The photoacoustic technique with gas-microphone registration was applied for the thermal diffusivity evaluation of the samples. Particularly, the amplitude frequency dependencies of photoacoustic response from the considered samples in the classical gas-microphone configuration were measured in the range from 10 Hz to 3 kHz. The simulation of the experimental dependencies with the use of appropriate model allowed us to evaluate thermal conductivity. It was found that the short time thermal annealing together with increasing annealing temperature leads to significant reduction of thermal transport in mesoporous silicon. On the opposite, the thermal properties of silicon nanowires remain unaffected.

INTRODUCTION

For decades, the miniaturization of electronic devices has become a characteristic and important feature in modern electronics [1]. The main goal of this trend is a cheap and safe design and further implementation of compact, lightweight and manageable devices. A significant number of these devices consists of operating components that have a critical nanoscale size. However, the miniaturizing of the devices significantly increases the density of its components, which leads to a steep increase of heat flows from microprocessor chips. Thus, there is growing demand regarding the emergence of on-chip hot spots and related safety issues regarding their subsequent use under the critical temperatures. Therefore, the efficiency and durability of nanoscale electronic devices operation strongly depend on the engineering of its building blocks with proven and stable properties.

Among silicon nanostructures, a great interest has recently been shown to the properties tuning of porous materials with different porosities and pore morphologies in a wide range of values [2–4]. However, bulk silicon surface is covered by silica film, and because porous silicon nanostructures have a large surface-to-volume area, therefore the presence of possible uncontrolled oxidation cannot be neglected even under the storage of the structures in ambient air. Moreover, it has been observed that during the annealing process the crystalline Si partially

Thermophysics 2019
AIP Conf. Proc. 2170, 020008-1–020008-7; https://doi.org/10.1063/1.5132727
Published by AIP Publishing. 978-0-7354-1917-9/$30.00

turns into SiO_2, and consequently the thermal and optical properties of the porous structure are changed and need to be regularly checked by diagnostic methods [5,6]. On the other hand, the control of porous nanostructures` surface chemistry through its intentional thermal oxidation is also indispensable to functionalize and stabilize its properties with the expectation of better reliability. Therefore, the main aim of this work is to study how thermal annealing affects the peculiarities of heat transport inside the porous silicon-based nanostructures with different morphology. Specifically, we focused on the sponge-like mesoporous silicon layer (PSi), produced by electrochemical etching, and the well-ordered silicon nanowire arrays (SiNWs), fabricated by metal-assisted chemical etching (MACE) of monocrystalline silicon wafer. We chose the photoacoustic technique because it is well adapted for the study of various porous materials [7–9].

MATERIALS AND METHOD

The PSi samples were prepared by electrochemical etching of a monocrystalline (100)-oriented boron-doped Si wafer in an electrolyte made of concentrated aqueous (49 %) HF and pure ethanol in a volume ratio of 1:1. Both thickness and porosity of PSi were adjusted by tuning the anodization current density and etching duration [10]. The elaboration conditions were chosen to fabricate mesoporous silicon with pore diameters in the range of 10-20 nm located on crystalline silicon substrate.

The SiNWs arrays were synthesized via the two step MACE process, as described in [11]. After the etching process, all the samples were carefully rinsed with pure ethanol and deionized water for several times and dried in the air at room temperature in order to remove the remaining electrolyte or metal catalyst from the pores.

Thermal annealing of the prepared PSi and SiNWs samples was carried out in dry air for 20 minutes at various temperatures, from 600°C up to 1000°C.

TABLE 1. Structural characteristics of the investigated samples.

Sample	Doping level, cm^{-3}	Porosity, %	The average thickness of porous layer, µm	c-Si substrate thickness, µm
PSi	10^{19}	60 ± 2	50 ± 1	465
SiNWs	10^{15}		20 ± 0.5	270

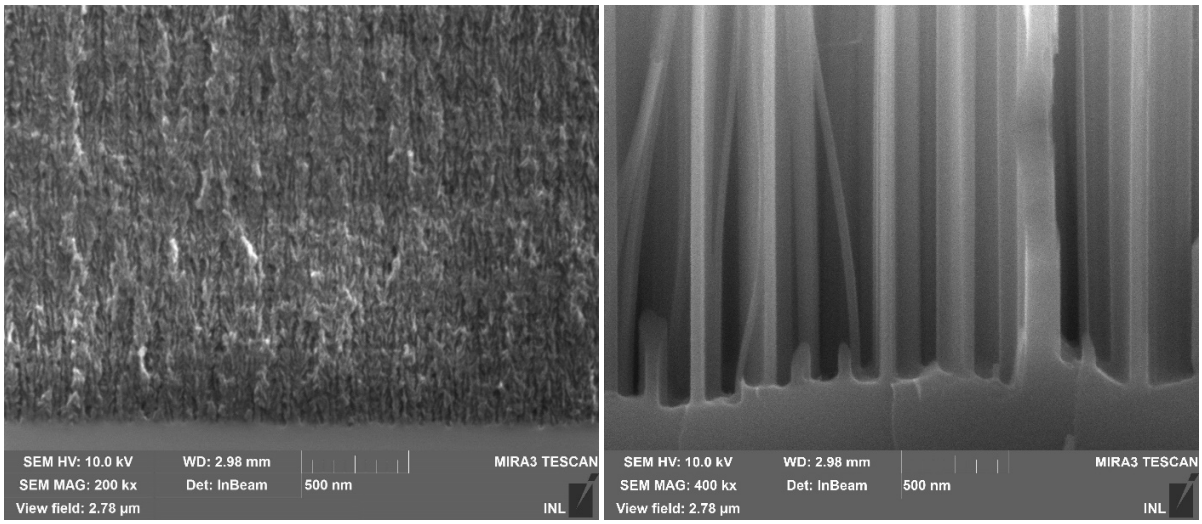

(a) (b)

FIGURE 1. SEM view of the prepared PSi (a) and SiNWs (b) structures.

The typical scanning electron images of the initial fractal-like PSi and ordered SiNWs arrays are presented on the Fig. 1. With the use of the images the diameters distribution in SiNWs arrays was to be in range from 50 to 200 nm with the averaged size equals to 120 nm. Additionally, with the use of SEM images we investigated the porosities of the samples. Nevertheless, these values were checked by the gravimetric method. The optical microscopy of annealed porous structures (see Fig. 2) reveals any considerable changes of its porous layer thickness

compared to the initial PSi and SiNWs samples. Table 1 summarizes the structural characteristics of porous silicon-based nanostructures investigated in the present work.

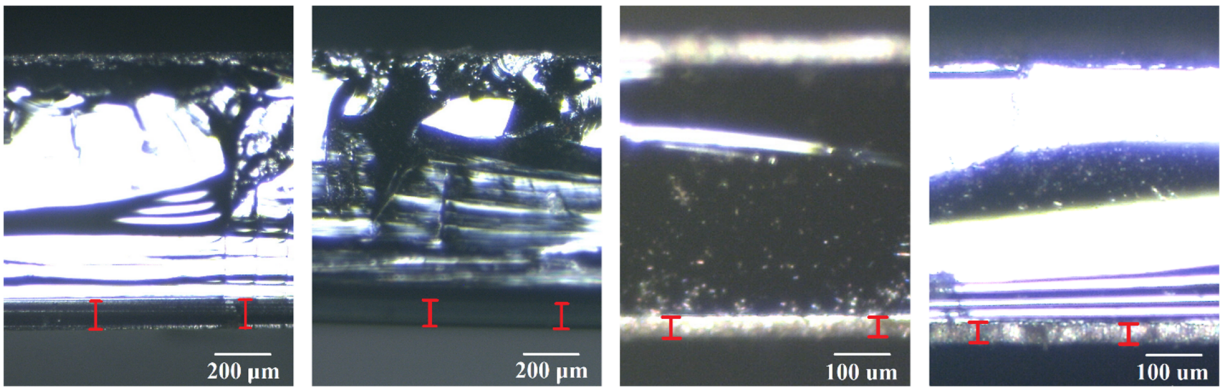

FIGURE 2. Cross-sectional images of PSi sample before (a) and after annealing at 1000 °C (b), and SiNWs sample before (c) and after annealing at 1000 °C (d), obtained by optical reflectivity microscopy.

Measurements of thermal diffusivity of the investigated samples were carried out at room temperature by a photoacoustic (PA) method with gas-microphone registration. The samples were alternately placed inside the classical PA cell and irradiated by the non-stationary electromagnetic radiation, as shown on Fig. 3. As an optical irradiation source, a green laser (λ=532 nm) with the output optical power ~ 100 mW was used. Its modulation was carried out by a square-wave signal generator. The amplitude of informative PA signal was recorded by the electret microphone and compared with the reference one by the lock-in amplifier (Unipan 232B).

We performed the measurements of the PA signal generated by the sample irradiation in the non-resonant low frequency range (from 20 Hz to 2250 Hz). The calibration of the PA cell was provided by the reference Si wafer with well-established thermal and optical properties.

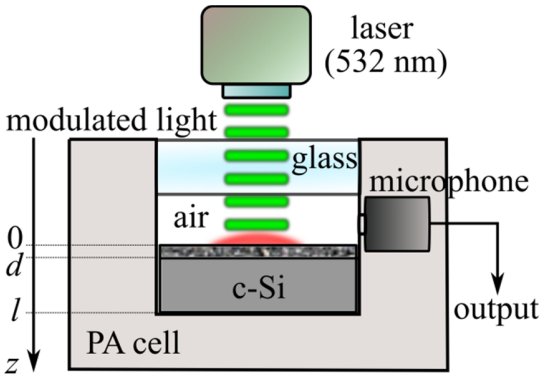

FIGURE 3. Sketch of the experimental setup employed for photoacoustic signal measurement

RESULTS AND DISCUSSION

The normalized by magnitude experimental amplitude-frequency characteristics (AFC) of the PA signal for PSi and SiNWs samples were obtained before and after thermal annealing with different temperatures (see Fig. 4). We can see on Fig. 4, that the oxidation of PSi samples leads to significant changes in its AFC. Moreover, the difference is more appreciable with the annealing temperature rising. Thus, a huge modification of the PA response registered

from PSi samples can be revealed. It can be related to oxidation of the samples hence they have significant surface-to-volume ratio.

On the other hand, thermal annealing impacts insignificantly the photoacoustic signal registered from SiNWs arrays because of its lower surface-to-volume ratio. Even after annealing at 1000 °C the AFC shows almost no difference.

The obtained experimental results were treated by using the thermal wave approach [11,12]: the spatial distribution of the variable component of temperature $\theta(z)$ induced in the two-layer structure under its periodical heating by modulated irradiation in one-dimensional approximation is described by the following heat conduction equations:

$$\begin{cases} \frac{d^2\theta}{dz^2} - \frac{i\omega}{D_1}\theta = -\frac{I\alpha}{\chi_1}\exp(-\alpha z) & 0 < z < d \\ \frac{d^2\theta}{dz^2} - \frac{i\omega}{D_2}\theta = 0 & d < z < l \end{cases} \quad (1)$$

where $D_i = \chi_i / (\rho_i c_i)$ is the thermal diffusivity of the layer i, index 1 and 2 corresponds to the porous Si layer and monocrystalline Si substrate, respectively, χ is the thermal conductivity, ρ is the density of material, c is the heat capacity, I is the absorbed light intensity, α is the optical absorption coefficient of porous layer, $\omega = 2\pi f$ is the cyclical frequency, f is the frequency, d is the average thickness of porous layer, l is the thickness of the entire structure.

The heat conduction equations with the temperature and flux continuity conditions at the sample layer surfaces allow us to evaluate the temperature distribution in the PA cell in terms of the optical, thermal, and geometric parameters of the investigated structure. Particularly, the solution of Eq. (1) in frame of the isolated top and bottom boundaries approximation can be expressed as follows:

$$\theta(z) = \begin{cases} A \cdot \exp(\sigma_1 z) + B \cdot \exp(-\sigma_1 z) - \frac{I\alpha \exp(-\alpha z)}{K_1(\alpha^2 - \sigma_1^2)} & 0 < z < d \\ C \cdot \exp(\sigma_2 z) + E \cdot \exp(-\sigma_2 z) & d < z < l \end{cases}, \quad (2)$$

where $\sigma_i = \sqrt{i\omega / D_i}$, A, B, C and E are the constants that can be defined from the boundary conditions and conditions of temperature and heat fluxes continuity at the interfaces between layers.

The acoustic waves that are generated in the adjacent to the samples surface gas, and propagated through the rest of the inner volume to the microphone, strongly depend on thermal and optical properties of the sample and can be described by the following equation:

$$U(\omega) \sim \rho(\omega) = \int_0^{-\infty} \theta(0) \cdot \exp\left(\sqrt{i\,\omega / D_{t\,g}}\, z\right) dz \quad (3)$$

where index g corresponds to gas, $\theta(0)$ is the temperature at the sample surface.

The fitting procedure of experimental AFCs with the theoretical ones was carried out by achieving the qualitative coincidence under varying thermal diffusivity and absorption coefficient parameters of porous layer (see Fig. 4). The experimentally obtained thermal diffusivity values of PSi and SiNWs samples versus annealing temperature are shown on Fig. 5.

Additionally, the right scale represents the recalculation of thermal diffusivity in thermal conductivity with rough approximation of constant (un-effecting on the annealing) volumetric heat capacity just to give general insight regarding order of magnitude. As one can see, the thermal conductivity values for the initial PSi and SiNWs samples are in good agreement with the results evaluated earlier for the same porous nanostructures [10,11,13,14].

Furthermore, Fig. 5 reveals a monotonic decreasing of thermal diffusivity of PSi with annealing temperature. At 1000 °C, the thermal diffusivity of PSi is approximately reduced by one order of magnitude in comparison with the initial sample. Such significant decreasing can be explained by important thermal oxidation of porous silicon with significant surface-to-volume ratio. On the opposite, thermal diffusivity of SiNW arrays remains constant, and it does not depend on annealing in this temperature/time range. Thus, SiNWs are promising to be applied as an efficient material that might improves heat and mass transfer through the solid/fluid interface [15].

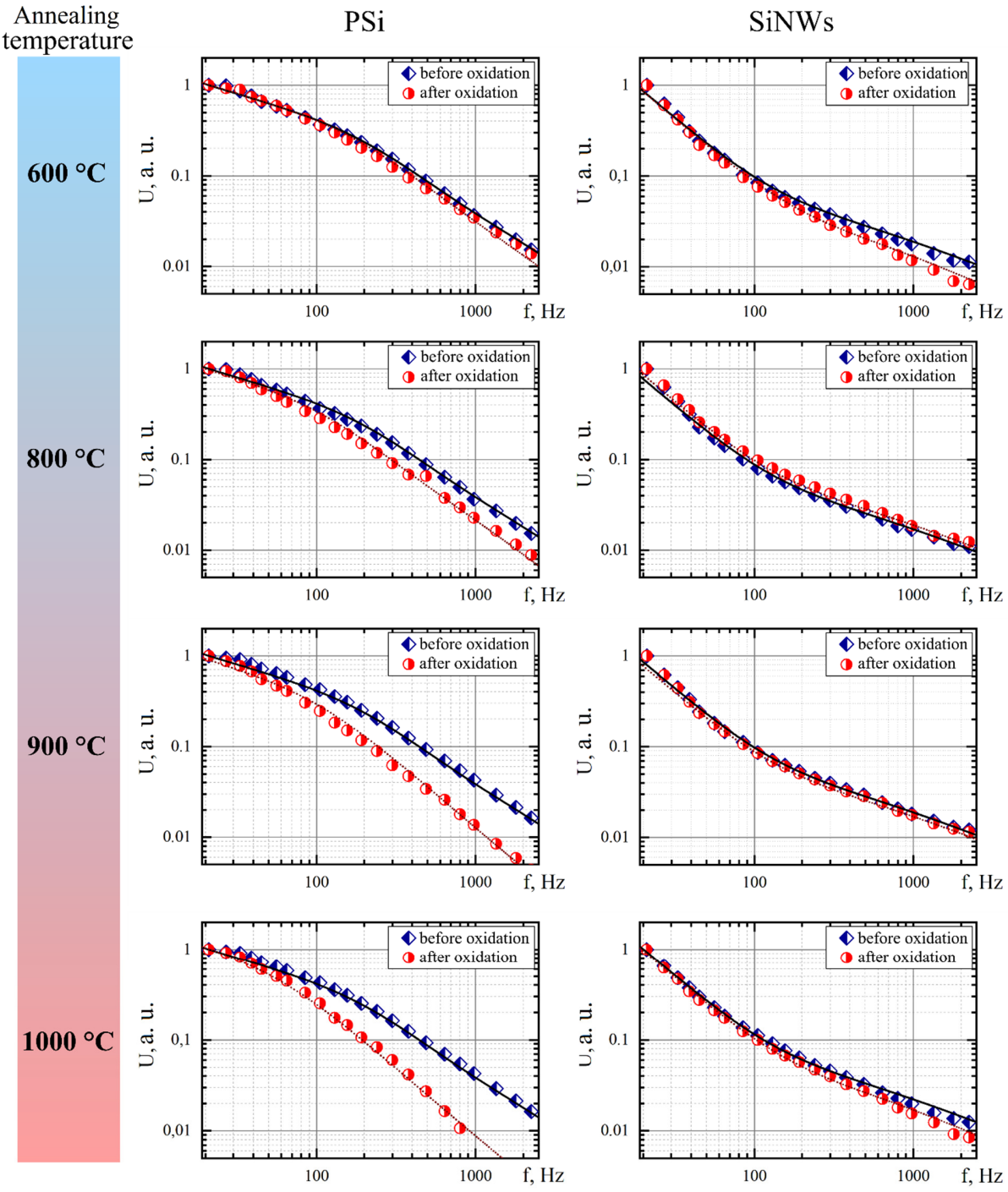

FIGURE 4. Experimentally normalized by magnitude amplitude-frequency dependencies of the obtained PA signal, detected by microphone for PSi samples (left) and SiNWs samples (right), before (rhombus) and after (circles) annealing process with different annealing temperatures. The solid and dashed lines correspond to the calculated AFC obtained from the temperature distribution simulations.

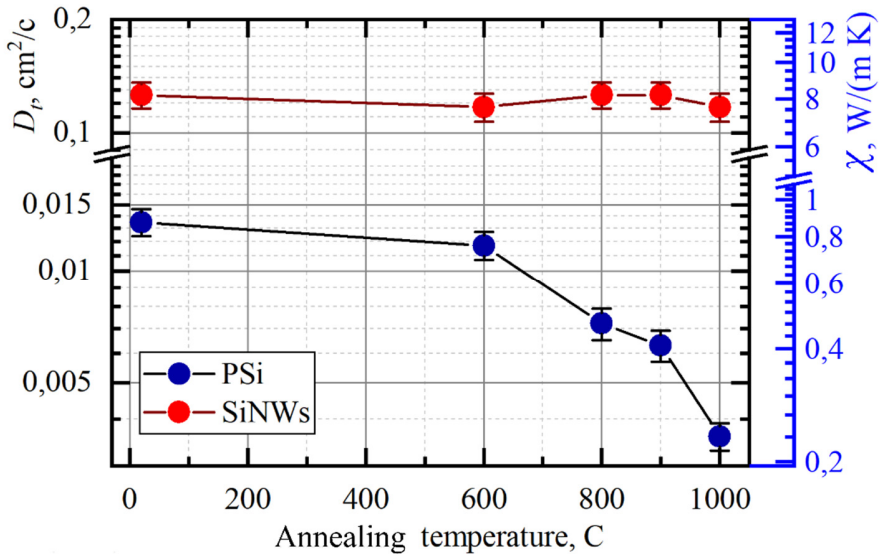

FIGURE 5. The experimentally obtained thermal diffusivity of PSi and SiNWs samples versus oxidation temperature. The secondary y-axis on the right shows the corresponding thermal conductivity values of the samples in case when the volumetric heat capacity remains constant.

CONCLUSIONS

In this paper, we analyzed the features of photoacoustic response registered from the porous silicon nanomaterials annealed under different temperatures as well as their thermal transport properties. The evolution of thermal properties of porous structures with dendrite-like fractal (porous silicon layer) and well-ordered (silicon nanowire arrays) morphologies were studied. Temperatures of annealing were chosen in diapason from 600 to 1000 °C. The dependence of thermal diffusivity of the samples on the temperature of annealing were measured by photoacoustic technique with gas-microphone registration.

It was revealed that thermal diffusivity of PSi layer significantly decreases with increasing the annealing temperature, while the weak dependence of the SiNWs thermal properties annealed under same temperature conditions is observed. Thus, thermal diffusivity of PSi can be significantly tuned under dry annealing process.

On the other hand, taken into account stability of SiNWs array, such materials can be used in different high temperature applications. Specifically, they can be used as an efficient substrate, for example, to improve heat and mass transfer across solid/fluid interface.

ACKNOWLEDGMENTS

This work has been partially funded by the CNRS Energy unit (Cellule Energie) through the project ImHESurNaASA. The publication contains the results obtained in the frames of the research work "Features of photothermal and photoacoustic processes in low-dimensional silicon-based semiconductor systems" (Ministry of Education and Science of Ukraine, state registration number 0118U000242). We want to acknowledge the partial financial support of the scientific pole EMPP of the University of Lorraine.

REFERENCES

1. 1. G. Korotchenkov, *Porous silicon from formation to application. Optoelectronics, microelectronics, and energy technology applications, Volume three* (CRC Press, Boca Raton, 2016) 421 p.
2. E. Dimaggio and G. Pennelli, Nanotechnology **29**, 135401 (2018).
3. B. Graczykowski, A. El Sachat, J.S. Reparaz, M. Sledzinska, M.R. Wagner, E. Chavez-Angel, Y. Wu, S. Volz,

Y. Wu, F. Alzina, and C.M. Sotomayor Torres, Nat. Commun. **8**, 4 (2017).
4. P. Lishchuk, A. Dekret, A. Pastushenko, A. Kuzmich, R. Burbelo, A. Belarouci, V. Lysenko, and M. Isaiev, Int. J. Therm. Sci. **134**, 317 (2018).
5. B. Remaki, D. Barbier, V. Lysenko, and S. Pe, Sensors Actuators A **99**, 13 (2002).
6. Y. Li, W. Liu, Y. Luo, M. Cui, and M. Li, Opt. Express **26**, A19 (2018).
7. D. Andrusenko, M. Isaiev, A. Tytarenko, V. Lysenko, and R. Burbelo, Microporous Mesoporous Mater. **194**, 79 (2014).
8. C.F. Ramirez-Gutierrez, J.D. Castaño-Yepes, and M.E. Rodriguez-García, J. Appl. Phys. **119**, 185103 (2016).
9. C.F. Ramirez-Gutierrez, J.D. Castaño-Yepes, and M.E. Rodriguez-García, J. Appl. Phys. **121**, 025103 (2017).
10. P. Lishchuk, D. Andrusenko, M. Isaiev, V. Lysenko, and R. Burbelo, Int. J. Thermophys. **36**, 2428 (2015).
11. P. Lishchuk, M. Isaiev, L. Osminkina, R. Burbelo, T. Nychyporuk, and V. Timoshenko, Phys. E Low-Dimensional Syst. Nanostructures **107**, 131 (2019).
12. A.I. Tytarenko, D.A. Andrusenko, A.G. Kuzmich, I. V. Gavril'chenko, V.A. Skryshevskii, M. V Isaiev, and R.M. Burbelo, Tech. Phys. Lett. **40**, 188 (2014).
13. M. Isaiev, O. Didukh, T. Nychyporuk, V. Timoshenko, and V. Lysenko, Appl. Phys. Lett. **101**, 011908 (2017).
14. K. Dubyk, A. Pastushenko, T. Nychyporuk, R. Burbelo, M. Isaiev, and V. Lysenko, J. Phys. Chem. Solids **126**, 267 (2019).
15. K. Voitenko, M. Isaiev, A. Pastushenko, D. Andrusenko, A. Kuzmich, V. Lysenko, and R. Burbelo, J. Phys. Conf. Ser. **785**, 012010 (2017).